

https://dspace.org/

Analyzing radiative heat on thirdgrade fluids over an expanding inclined sheet subject to higherorder chemical reaction An overlapping grid spectral quasilinearization approach

Titilayo Agbaje; F Oluwaseun; S Mishra; R Baithalu; S Panda

https://hdl.handle.net/10539/47316
DOAJ

Downloaded from a DSpace repository. https://dspace.org/

Partial Differential Equations in Applied Mathematics 13 (2025) 101098

Contents lists available at ScienceDirect

Partial Differential Equations in Applied Mathematics

journal homepage: www.elsevier.com/locate/padiff

Analyzing radiative heat on third-grade fluids over an expanding inclined sheet subject to higher-order chemical reaction: An overlapping grid spectral quasilinearization approach

Titilayo M Agbaje [a], Folarin Oluwaseun [b], S.R. Mishra [c], Rupa Baithalu [c], Subhajit Panda [d,*]

[a] School of Computer Science and Applied Mathematics, University of the Witwatersrand, Johannesburg, Private Bag 3, Braamfontein, 2050, South Africa
[b] School of Mathematics, Statistics, and Computer Science, University of the KwaZulu-Natal, Private Bag X01, Scottsville, Pietermaritzburg 3209, South Africa
[c] Department of Mathematics, Siksha 'O' Anusandhan Deemed to be University, Bhubaneswar, Odisha 751030, India
[d] Centre for Data Science, Department of Computer Science and Engineering, Siksha 'O' Anusandhan Deemed to be University, Bhubaneswar, Odisha 751030, India

ARTICLE INFO

Keywords:
Third-Grade fluid
Free convection
Radiative heat
Viscous dissipation
Higher-order chemical reaction
Over lapping grid spectral quasilinearization method

ABSTRACT

Higher-order chemical reactions significantly enhance the concentration of the fluid indicating its vital role in processes involving radiative species. Therefore, the observation shows its important practical applications in industrial processes such as polymer extrusion, in which heat transfer properties are useful in the production of quality products. The proposed study emphases on the free convection of a third-grade fluid via an inclined expanding sheet for the influence of radiative heat and higher-order chemical reactions. However, the analysis incorporates the influence of viscous dissipation that is significant in determining the thermal behavior of the fluid. Further, the proposed flow phenomena governed by the set of partial differential equations are transformed into ordinary ones by the operating of suitable similarity rules. The transformed equations equipped with characterizing parameters are handled by a numerical technique known as the over lapping grid spectral quasilinearization method. The quantitative behavior of the factors intricate in it is deployed graphically and described briefly. However, the important outcomes of the study are; Richardson number is useful in enhancing the fluid momentum whereas the impact is reversed for the temperature and concentration distribution. Further, increasing heavier species i.e., Schmidt number attenuates the concentration profile.

1. Introduction

Since fluid dynamics has so many applications in so many different industries and technical domains, studying fluid flow across expanding surfaces is important. In metal forming, where it helps produce components with precise dimensions and properties necessary for the automotive, aerospace, and construction industries, as well as in polymer extrusion, where controlling material behaviour as it exits the die ensures product uniformity and quality, this phenomenon is critical. Designing efficient medical equipment and drug delivery systems is essential to improve patient outcomes in biomedical engineering. This requires a solid grasp of fluid flow. Fluid dynamics insights improve sustainability and efficiency in environmental engineering applications such as wastewater treatment and pollution management. This research helps the automotive and aerospace industries by improving the aerodynamic vehicle designs that increase performance and fuel efficiency. Moreover, fluid flow studies are essential to chemical and process engineering because they help optimise heat exchangers, reactors, and separation units, which in turn results in more productive industrial processes. Fundamentally, advances in our knowledge of fluid flow across expanding surfaces are what propel technological innovation, economic efficiency, and the creation of long-term solutions to today's problems. Sandeep and Sulochana[1] analyzed heat transference phenomena in non-Newtonian fluids over an expanding surface. In their concluding remark, they proposed that Jeffrey nanofluids exhibited superior thermal transmission performance compared to Maxwell as well as Oldroyd-B nanofluids. An analytical approach is exhibited by Abolbashari et al.[2] focusing on a situation involving an elastic sheet under a momentum slip constraints. Shit et al.[3] proposed an enquiry on the imposition of external heat source/sink on the magnetohydrodynamic unsteady flow within a boundary layer.

* Corresponding author.
E-mail addresses: titilayoagbaje@gmail.com (T.M. Agbaje), folarino987@yahoo.com (F. Oluwaseun), satyaranjan_mshr@yahoo.co.in (S.R. Mishra), rupadhananjaygarnaik@gmail.com (R. Baithalu), spanda.math@gmail.com (S. Panda).

https://doi.org/10.1016/j.padiff.2025.101098

Available online 28 January 2025
2666-8181/© 2025 The Author(s). Published by Elsevier B.V. This is an open access article under the CC BY-NC-ND license (http://creativecommons.org/licenses/by-nc-nd/4.0/).

Nomenclature

U_w	stretching velocity (m/s)	α	Inclined angle
T_w	temperature of the sheet (K)	*Ri*	Richardson number
C_w	concentration of surface	*M*	magnetic term
$\alpha_1,\alpha_2,\beta_3$	material moduli	*Sc*	Schmidt number
K_0	chemical reaction	*K*	cross viscous term
Q_0	heat source (J)	*R*	Chemical reaction parameter
δelectrical conductivity	electrical conductivity(S/m)	*Hs*	heat source term
C_p	specific heat capability (J/Kg.K)	Re	Reynolds number
μ	dynamic viscosity (N.s/m^2)	*Gr*	Grashof number
Pr	Prandtl number	*L*	viscoelastic parameter
ν	kinematic viscosity (m^2/s)	*Nr*	Radiation parameter
N	buoyancy ratio term	C_f	drag force (N)
D_m	thermal diffusivity(m^2/s)	*Sh*	Sherwood number
α_m	mass diffusivity(m^2/s)	*Nu*	Nusselt number
q_r	radiative heat flux	q_w	heat flux
		q_m	mass flux
		τ_w	shear stress

The movement of a fluid-solid particle mixture is inherently complex and affected by numerous factors. To gain a clearer understanding of these intricate flows, the mixture is frequently modeled as a non-Newtonian fluid. Extensive research has been devoted to analyzing diversified flow properties considering different non-Newtonian fluids, such as coal slurries. Thermal transportation, in particular, is crucial for the efficient management and processing of these fluids. Ariel[4] explored the circukation stability of a 3rd grade liquid via a permeable flat channel, while Ellahi and Riaz[5] examined with variable viscosity, including an analysis of the fluid's heat diffusion properties. Mahanthesh and Joseph[6] considered the stable flow charecteristic of a 3rd grade liquid via a pressure-type die while nanoparticles were present. The fluid was treated as dissipative, maintaining constant properties throughout the study. For further exploration of non-Newtonian (third-grade) fluids, recent and pioneering literature can be referred to in Refs. .[7–11] An interesting work examined by Reddy et al.[12] that the role of the Prandtl number on the gravitational flow around a uniformly heated, rotating cylinder placed vertically. Baithalu et al.[13] deliberated the movement of a magneto-polar hybrid nanomaterial on an enlarging surface. The work highlighted the importance of couple stresses and shear rates in determining flow behavior.

In industries where high temperatures are essential, such metallurgy, glass manufacture, and ceramics, thermal radiation is often used. In these domains, radiant heat transfer is the means by which heaters, kilns, and furnaces reach and hold the temperatures necessary for material processing. Mishra and Upreti[14] have considered the behavior of the dissipative heat along with the insertion of heat source/sink by considering various hybrid nanofluid. They proposed hybrid nanofluids are silver-Magnesium oxide/water and Magnetite-Cobalt ferrite/water–ethylene glycol for the interpretation of chemical reactions related to the Buongiorno model. Moreover, the numerical simulation is then attained via the shooting method combined with "*Runge–Kutta–Fehlberg (RKF45)*" algorithm in MATLAB. Mishra and Kumar[15] studied the momentum and thermal ability of MHD Ag/H_2O nanofluid influenced by incorporating dissipative heat combined with Joule and viscous over an expanding cylinder, considering suction/injection and slip surface conditions. Finally, the subsequent nonlinear equations are solved via the "*Runge–Kutta–Fehlberg (RKF) fourth–fifth order*" numerical method through the shooting algorithm. The study of Mishra[16] examined the momentum of a tri nanoliquid, influenced by buoyancy effects across distinct geometries. Also, incorporates the association of quadratic radiating heat and an irregular heat source/sink. The model development is based on the "CattaneoChristov theory". Aly et al[17] explored convective heat transmission utilizing a hybrid nanomaterial on a surface undergoing nonlinear elastic sheet, taking radiative effects into account. Akram et al[18] elaborated the heat temmision capabilities of Ag nanofluids flowing through a microchannel under electroosmotic pumping, as well as water-based hybrid nanomaterial. Alhussain et al[19] examined blood-based thin-film variable viscosity Casson hybrid nanofluid flow system. Wang et al[20] analyzed a tri-hybridized blend in ethylene glycol with varying thermal conductivity and diffusion, employing the non-Fourier's theory technique. Singh et al.[21] explored the flow and thermal behavior of a tri-hybrid nanofluid (TiO_2-Al_2O_3--MoS_2/kerosene oil) around a circular cylinder with a sinusoidal radius, highlighting its superior heat conduction performance compared to conventional hybrid nanofluids. The governing partial differential equations are solved using the bvp4c solver. The findings emphasize the significant influence of nanoparticle shape on heat transfer efficiency. Maheswari et al.[22] srudied a models for the bioconvective flow of a Casson nanofluid over a stretching sheet, where the nanofluid contains aerobic microorganisms and has a nanoparticle concentration below 1%. The surface of the sheet is subjected to thermal radiation and suction effects. To analyze the flow dynamics, the bvp4c solver is applied to the governing equations. A comparative analysis is conducted between Newtonian and Casson nanofluid flows, examining the impact of various active parameters on flow behavior. Singh et al.[23] studied the nonlinear convective flow characteristics (velocity and temperature profiles) of a Casson hybrid nanofluid (HNF) in the vicinity of a wedge and cone embedded within a porous medium. A strong, uniform magnetic field is applied to the object's surface, and the CattaneoChristov model is employed to incorporate the time lag factor in the heat transfer process. The energy equation formulation takes into account several key influences, including viscous dissipation, a nonuniform heat source/sink, thermal radiation, and Ohmic heating induced by the magnetic field. The governing equations are solved using the bvp4c solver.

1.1. Focus point of the proposed investigation

- The literature survey on the relating subject lead to find the followings as the measure objective of the study to;
- Analyze the free convection effect on the motion of third-grade non-Newtonian fluid via an inclined elastic surface.
- Examine the effectiveness of the inclusion of radiating heat affecting the energy transport phenomena of third grade fluid.
- Evaluate the ipact of dissipative heat as well as the higher-order chemical reaction on the flow characteristic.
- Execute the governing transfored model problem by using a suitable numerical technique called the quasilinearization method.

1.2. Novel characteristic of the study

The following approach shows the proposed work is novel;

- The proposed investigation explores the interaction between thermal radiation and higher-order chemical reactions in a third grade fluid.
- Dissipative heat along with thermal raiation provides significant characteristics in various industrial processes.
- The use of similarity transformations to renovate the governing PDEs into ODEs, followed by numerical solutions using the spectral quasilinearization method.

2. Description of the model

Let us assume a time independent movement of third grade fluid via an inclined permeable expanding surface. The free convective flow equipped with both the buoyant forces such as the solutal and thermal buoyancy effects enriches the flow phenomena. The main flow direction is act on the vertical x-axis and the normal direction is y. The variable magnetic field B(x) with magnetic strength is executed towards the transverse direction of the main flow. The sheet temperature and concentration are proposed to be $T_w(x)$and$C_w(x)$correspondingly and consequently the ambient state constraints are T_∞ and C_∞ (Fig. 1).

Let assume the following assumptions:

v Steady flow
v Incompressible flow
v 3rd grade 2-Dimensional flow
v Viscous flow
v Lorentz force
v Chemical reactions effect on the mass transmission.

The following fundamental equations have been established by using the aforementioned assumptions:

$$\partial_x u + \partial_y v = 0, \tag{1}$$

$$\left.\begin{aligned} u\partial_x u + v\partial_y u = \nu\partial_{yy}u + \frac{\alpha_1}{\rho}\left(u\partial_{xyy}u + \partial_x u\partial_{yy}u + 3\partial_y u\partial_{yy}u + \nu\partial_{yyy}u\right) + 2\frac{\alpha_1}{\rho}\partial_y u\partial_{yy}u + 6\frac{\beta_3}{\rho} \\ \left(\partial_y u\right)\left(\partial_{yy}u^2\right) + g(T-T_\infty)\beta_T\cos\alpha + g(C-C_\infty)\beta_c\cos\alpha - \frac{\sigma B(x)^2}{\rho} \end{aligned}\right\} \tag{2}$$

$$u\partial_x T + v\partial_y T = \alpha\partial_{yy}T + \frac{\mu}{\rho c_p}\left(\partial_y u\right)^2 + \frac{Q_0}{\rho c_p}(T-T_\infty) - \frac{\partial_y q_r}{\rho c_p}, \tag{3}$$

$$u\partial_x C + v\partial_y C = D_m\partial_{yy}C - k_r(C-C_\infty)^n. \tag{4}$$

The surface restriction related to basic equations are:

$$\left.\begin{aligned} &at\ \ y=0: [u,v,T,C] = \left[U_w = U_0 e^{\frac{x}{L}}, 0, T_w(x) = T_\infty + T_0 e^{\frac{x}{L}}, C_w(x) = C_\infty + C_0 e^{\frac{x}{L}}\right] \\ &as\ \ y\to\infty: \left[u, \frac{\partial u}{\partial y}, T, C\right] = [0, 0, T_\infty, C_\infty] \end{aligned}\right\} \tag{5}$$

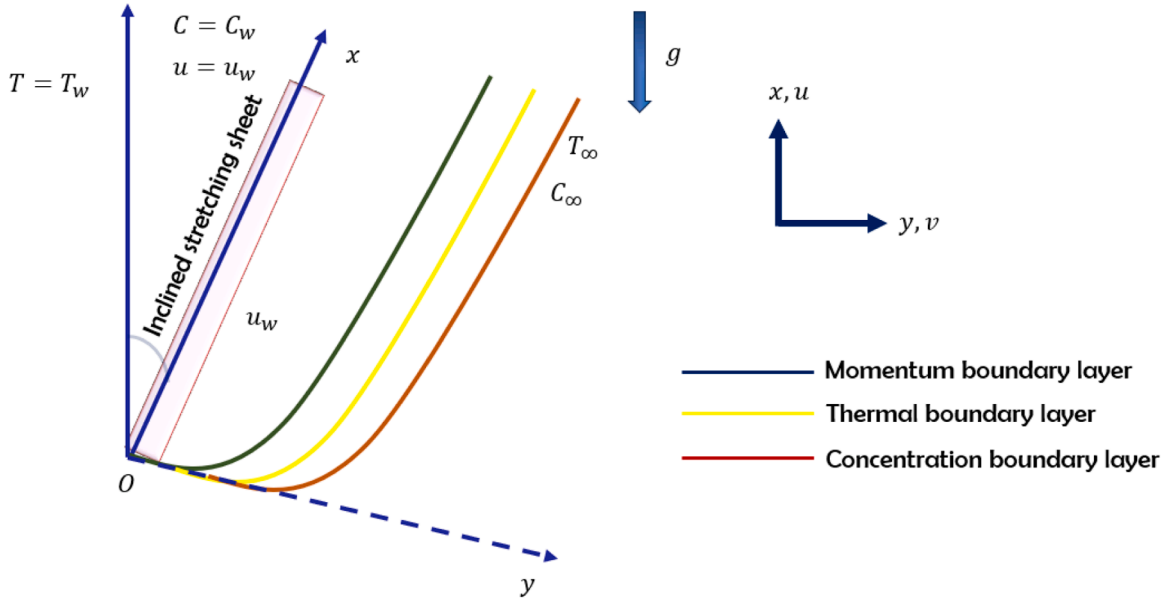


Fig. 1. Flow model.

Here $q_r = -\frac{4\sigma^*}{3k^*}\frac{\partial T^4}{\partial y}$is radiative heat flux, and $B(x) = B_0 e^{\frac{x}{L}}$is the magnetic effect.

However, the plate velocityU_w, Temperature $T_w$and Concentration $C_w$are considered as variable whereas the ambient velocity ceases to 0 with ambient temperature $T_\infty$and C_∞ respectively.

The following are the similarity variables used for the transformation as:

$$\left.\begin{aligned} u = U_0 e^{\frac{x}{L}} f'(\eta), v = \sqrt{\frac{\nu U_0}{2L}}(f(\eta)) + \eta f'(\eta))e^{\frac{x}{L}}, \ \eta = \sqrt{\frac{U_0}{2L\nu}} y e^{\frac{x}{L}}, \\ T = T_\infty + T_0 e^{\frac{x}{L}}\theta(\eta), \ C_w = C_\infty + C_0 e^{\frac{x}{L}}\phi(\eta). \end{aligned}\right\} \tag{6}$$

By implementing Eq. 6 in Eqs. (2-5) one can get,

$$f''' + ff'' - 2f'^2 + 2R_i(\theta + N\phi)\cos\alpha + K\left(6f'f''' - ff^{iv} - 2\eta f''f''' - 9f''^2\right) - L\left(3f''^2 + \eta f''f'''\right) + 3\beta Ref''^2 f''' - Mf' = 0, \tag{7}$$

$$(1+Nr)\theta'' + Pr\left(f\theta' - f'\theta + Ecf''^2 + Hs\theta\right) = 0, \tag{8}$$

$$\phi'' + Sc(f\phi' - f'\phi) - ScR\phi^n = 0, \tag{9}$$

renovated conditions:

$$\left.\begin{aligned} \phi(\eta) = 1, \ \theta(\eta) = 1, \ f'(\eta) = 1, f(\eta) = 0, \quad at \ \ \eta = 0 \\ \phi(\eta)\to 0, \theta(\eta)\to 0, f''(\eta)\to 0, f'(\eta)\to 0 \ \text{as} \ \ \eta\to\infty \end{aligned}\right\}. \tag{10}$$

The dimension less parameters we obtained from modified equations are as follows:

$$Ri = \frac{Gr}{\mathrm{Re}^2}, N = \frac{B_c C_0}{\mathrm{Re}^2}, L = \frac{\alpha_2 U_0 e^{\frac{x}{L}}}{2\rho\nu L}, K = \frac{\alpha_1 U_0 e^{\frac{x}{L}}}{\mathrm{Re}^2}, \beta = \frac{\beta_2 U_0 e^{\frac{x}{L}}}{\rho\nu L}, M = \frac{2\sigma{\beta_0}^2}{\rho U_0}, \mathrm{Pr} = \frac{\nu}{\alpha}, Sc = \frac{\nu}{D_m}, R = \frac{2k_1 L}{U_0 e^{\frac{x}{L}}},$$
$$Hs = \frac{Q_0}{\rho C_p U_0}, Re = \frac{U_0 L}{\nu}, Gr = \frac{g\beta_T(T_w - T_\infty)L^3}{\nu^2}, Nr = \frac{16\sigma^* T_\infty^3}{3k^* k_f}.$$

The important physical engineering coefficients i.e., drag force; Sherwood number and Nusselt number are described as:

$$C_f = \frac{\tau_w}{\rho U_w^2}, \ Sh = \frac{q_m x}{D_m(C - C_\infty)}, \ Nu = \frac{q_w x}{k(T - T_\infty)}. \tag{11}$$

Where

$$\left.\begin{aligned} q_w = -k(\partial_y T) - q_r, \ q_m = -D_m(\partial_y C) \ \ \text{at} \ \ y = 0, \\ \tau_w = \left(\partial_y u + \frac{\alpha_1}{\mu}\left(2\partial_x u\partial_y u + \nu\partial_{yy}u + u\partial_{xy}u\right) + \frac{2\beta_3}{\mu}(\partial_y u)^2\right). \end{aligned}\right\} \tag{12}$$

The non-dimensional form of engineering coefficients present in Eq. (11) is:

$$C_{fL} = \frac{2}{\sqrt{Re_L}}\left(f''(0) + K(3f''(0)f'(0) - f(0)f''(0)) + 2\beta Re_x f''^2(0)\right),$$
$$Re_L^{-\frac{1}{2}} Nu_L = -(1+Nr)\theta'(0), \ Re_L^{-\frac{1}{2}} Sh_L = -\phi'(0).$$

Where *Re*is the Reynolds number.

3. Overlapping grid spectral Quasi-linearisation method

Overlapping Grid Spectral Quasi-linearisation (OSQLM) is utilized in this study to numerically solve a set of ODEs specified in Eqs. (7-9) concern to the surface constraints specified in Eq. (10). This solution approach is iterative and involves dividing the domain into several sub-domain's grids. It incorporates various techniques including quasi-linearization, "*modified Chebyshev spectral collocation*", and "*Lagrange interpolation*" with "*Gauss-Lobatto grid points*". By employing the conventional "*Spectral Quasilinearisation Method (SQLM)*", superior stability is ensured with a reduced number of grid points, while maintaining appropriateness, correctness, and decreased computation time compared to traditional numerical techniques likely "*shooting method*", "*Runge-Kutta method*", and "*Keller Box method*" as reported by Mkhatshwa and Khumalo[26] and Mkhatshwa.[27] The utilization of SQLM on overlapping grids significantly expands its efficiency in terms of steadiness for larger sub-domains with lesser grid points, accurateness, and computational time. This enhancement is attributed to the sparse coefficient matrices involved in the overlapping grid spectral quasi-linearisation method, which leads to more efficient matrix inversion and vector multiplication.

The finite solution domain in this case is characterized by a truncated integration distance $I = [0, \eta]$, which is subsequently segmented into p overlapping sub-domains deliberated as:

$$I_l = \left[\eta_0^l, \eta_{M_\eta}^l\right], l = 1, 2, 3, \ldots p.$$

Considering $M_\eta + 1$ collocation point for the subintervalsI_l, the length of the domain is given by

$$L = \frac{\eta}{p + (1-p)\frac{\left(1 - \cos\left(\frac{\pi}{M_\eta}\right)\right)}{z}}. \tag{13}$$

The length of the domain, is determined via the "*Gauss-Lobatto collocation points*" given by$z_i = \cos\left(\frac{\pi_i}{M_\eta}\right), I = 0, 1, 2, 3, \ldots M_\eta,$

$$= \frac{L}{2}\left(1 - \cos\left(\frac{\pi_i}{M_\eta}\right)\right)(1-p) + pL, .$$

In the current study, where the problem is defined on an infinite domain, $\eta = \infty$.

Next, we solve Eqs. (6)–(10) in each sub-interval, I_l as

$$\begin{aligned} &\frac{d^3 f^{(l)}}{d\eta^3} + f^l\frac{d^2 f^{(l)}}{d\eta^2} - 2\frac{df^{(l)}}{d\eta}\frac{df^{(l)}}{d\eta} + 2R_i(\theta^l + N\phi^l)\cos\alpha + 6K\frac{df^{(l)}}{d\eta}\frac{d^3 f^{(l)}}{d\eta^3} \\ &-Kf^l\frac{d^4 f^{(l)}}{d\eta^4} - 2K\eta\frac{d^2 f^{(l)}}{d\eta^2}\frac{d^3 f^{(l)}}{d\eta^3} - 9K\frac{d^2 f^{(l)}}{d\eta^2}\frac{d^2 f^{(l)}}{d\eta^2} - 3L\frac{d^2 f^{(l)}}{d\eta^2}\frac{d^2 f^{(l)}}{d\eta^2} \\ &-\eta L\frac{d^2 f^{(l)}}{d\eta^2}\frac{d^3 f^{(l)}}{d\eta^3} + 3\beta Re\frac{d^2 f^{(l)}}{d\eta^2}\frac{d^2 f^{(l)}}{d\eta^2}\frac{d^3 f^{(l)}}{d\eta^3} - M\frac{df^{(l)}}{d\eta} = 0 \end{aligned} \tag{14}$$

$$(1+Nr)\frac{d^2\theta^{(l)}}{d\eta^2} + Prf^{(l)}\frac{d\theta^{(l)}}{d\eta} - Pr\frac{df^{(l)}}{d\eta}\theta^{(l)} + PrEc\frac{d^2 f^{(l)}}{d\eta^2}\frac{d^2 f^{(l)}}{d\eta^2} + PrHs\theta^{(l)} = 0, \tag{15}$$

$$\frac{d^2\phi^{(l)}}{d\eta^2} + Scf^{(l)}\frac{d\phi^{(l)}}{d\eta} - Sc\frac{df^{(l)}}{d\eta}\phi^{(l)} - ScR\phi^{n(l)} = 0. \tag{16}$$

In tackling Eqs. (14)-(16), we need to linearize the nonlinear ODEs

via the Quasilinearization Method (QLM). This method operates under the assumption that the disparity between approximate solutions in consecutive iterations is negligible. When applied to Eqs. (14)-(16), the QLM produces the subsequent iterative sequence of linear Ordinary Differential Equations (ODEs):

To achieve these solutions, we employ a linearization approach, utilizing the quasilinearization technique, as typically done in the conventional SQLM, that is;

$$\alpha_{0,r}f^{iv}_{r+1} + \alpha_{1,r}f'''_{r+1} + \alpha_{2,r}f''_{r+1} + \alpha_{3,r}f'_{r+1} + \alpha_{4,r}f_{r+1} + \alpha_{5,r}\theta_{r+1} + \alpha_{6,r}\phi_{r+1} = R_f, \tag{17}$$

$$\omega_{0,r}\theta''_{r+1} + \omega_{1,r}\theta'_{r+1} + \omega_{2,r}\theta_{r+1} + \omega_{3,r}f''_{r+1} + \omega_{4,r}f'_{r+1} + \omega_{5,r}f_{r+1} = R_\theta, \tag{18}$$

$$\Gamma_{0,r}\phi''_{r+1} + \Gamma_{1,r}\phi'_{r+1} + \Gamma_{2,r}\phi_{r+1} + \Gamma_{3,r}f'_{r+1} + \Gamma_{4,r}f_{r+1} = R_\phi, \tag{19}$$

Associate with the assumed variable coefficients specified as:

$$\alpha_{0,r} = -Kf_r, \quad \alpha_{1,r} = 1 + 6Kf'_r - 2K\eta f''_r - \eta Lf''_r + 3\beta Ref''^2_r,$$

$$\alpha_{2,r} = f_r - 2K\eta f'''_r - 18Kf''_r - 6Lf''_r - \eta Lf'''_r + 6\beta Ref''_r f'''_r,$$

$$\alpha_{3,r} = -4f'_r + 6Kf'''_r - M, \alpha_{4,r} = f''_r - Kf^{iv}_r, \alpha_{5,r} = 2R_i\cos\propto, \alpha_{6,r} = 2NR_i\cos\propto.$$

$$\varpi_{0,r} = 1 + Nr, \varpi_{1,r} = Prf_r, \varpi_{2,r} = -Prf'_r + PrHs, \varpi_{3,r} = 2PrEcf''_r, \varpi_{4,r} = -Pr\theta_r, \varpi_{5,r} = Pr\theta'_r.$$

$$\Gamma_{0,r} = 1, \Gamma_{1,r} = Scf_r, \Gamma_{2,r} = -Scf'_r - ScnR\phi^{n-1}_r, \Gamma_{3,r} = -Sc\phi_r, \Gamma_{4,r} = Sc\phi'_r$$

The right-hand side of Eqs. (17-19) are defined as:

$$R_f = \alpha_{0,r}f^{iv}_r + \alpha_{1,r}f'''_r + \alpha_{2,r}f''_r + \alpha_{3,r}f'_r + \alpha_{4,r}f_r + \alpha_{5,r}\theta_r + \alpha_{6,r}\phi_r - V_f,$$

$$R_\theta = \varpi_{0,r}\theta''_r + \varpi_{1,r}\theta'_r + \varpi_{2,r}\theta_r + \varpi_{3,r}f''_r + \varpi_{4,r}f'_r + \varpi_{5,r}f_r - V_\theta,$$

$$R_\phi = \Gamma_{0,r}\phi''_r + \Gamma_{1,r}\phi'_r + \Gamma_{2,r}\phi_r + \Gamma_{3,r}f'_r + \Gamma_{4,r}f_r - V_\phi,$$

where,

$$V_f = f'_r{}'' + f_rf''_r - 2f'^2_r + 2R_i(\theta_r + \phi_r)\cos\alpha + K\left(6f'_rf''_r - f_rf^{iv}_r - 2\eta f'_rf'''_r - 9f'^2_r\right), \\ - L\left(3f''^2_r + \eta f''_rf'''_r\right) + 3\beta Ref'^2_rf'''_r - Mf'_r$$

$$V_\theta = (1+Nr)\theta''_r + Pr(f_r\theta'_r - f'_r\theta_r + Ecf''^2_r + Hs\theta_r,$$

$$V_\phi = \phi''_r + Sc\left(f_r\phi'_r - f'_r\phi_r - R\phi^n_r\right).$$

The current problem is defined in the domain[0, ∞], then each interval $I_l = \left[\eta^l_0, \eta^l_{M\eta}\right]$ is altered into $z\varepsilon[-1, 1]$ via the linear transformation$\eta^l_i = \frac{L}{2}(z_i + 1)$, $z_i = \cos\left(\frac{\pi i}{M\eta}\right)$. Before applying the "*spectral collocation method*" to the sub-intervals, we first estimate the first derivative given as:

$$\frac{dH^l}{dx} = \sum_{j=0}^{M_\eta} D^l_{i,j}H^l(z_j),$$

where, $D^l_{i,j} = \frac{2}{\eta^l_{M_\eta} - \eta_0}\breve{D}_{i,j}, i = 0, 1, 2, \ldots M_\eta.$ and $H^l(z_j) = [f^l(z_j), g^l(z_j), \theta^l(z_j), \phi^l(z_j)]$.

The term $\breve{\boldsymbol{D}}_{i,j}$ signifies the 1st order differential operator in a single domain [− 1, 1]. Likewise, the *qth* order derivative at the sub-interval I_l is obtained as:

$$\frac{d^qH^l}{dz^q} = \sum_{j=0}^{M_\eta}\left[D^{(l)}_{i,j}\right]^qH^l(z_j), i = 0, 1, 2, \ldots M_\eta. \tag{20}$$

Next, we derive the derivatives of the undetermined functions in a system of equations, which have the following definitions:

$$\left.\begin{aligned} \Delta_{11}\breve{f}_{r+1} + \ + \Delta_{12}\breve{\theta}_{r+1} + \Delta_{13}\phi_{r+1} = R^l_f, \\ \Delta_{21}\breve{f}_{r+1} + \ + \Delta_{22}\breve{\theta}_{r+1} + \Delta_{23}\phi_{r+1} = R^l_\theta, \\ \Delta_{31}\breve{f}_{r+1} + \ + \Delta_{32}\breve{\theta}_{r+1} + \Delta_{33}\phi_{r+1} = R^l_\phi \end{aligned}\right\} \tag{21}$$

Each matrix $\Delta_{\zeta,\sigma}(\zeta = 1, 2, 3; \sigma = 1, 2, 3)$ is of size $(M_\eta + 1) \times (M_\eta + 1)$ and R^l_f, R^l_g, R^l_θ, and $R^l_\phi$are vectors each of size $(M_\eta + 1) \times 1$.

A less dense matrix system is obtained after implementing the surface constraints as defined in Oluwaseun et al. .[28] After then, the system is solved with suitable initially guesses meeting the boundary constraints. The initial guesses for the current model are:

$$f_0(\eta) = 1 - e^{-\eta}, \theta_0(\eta) = e^{-\eta}, \phi_0(\eta) = e^{-\eta}.$$

4. Parametric analysis

This study scrutinizes the free convection flow of a third-grade fluid via an inclined stretched sheet while taking higher-order chemical processes and radiating heat into account. The study also incorporates the substantial influence of viscous dissipation on the thermal behavior of the fluid. The basic PDEs describing the flow phenomena are transformed into a set of ODEs via appropriate similarity transformations. These transformed equations, characterized by various parameters, are solved numerically via the "*spectral quasilinearization method*".

In this section of the study, we present the numerical results obtained using the "*Overlapping Spectral Quasilinearization Method (OSQLM)*". These findings are generated through MATLAB codes, showcasing flow profiles under varying physical parameters. The specific value chosen for the boundary at $\eta_\infty = 10$ and the number of collocation points, set at $M_\eta = 30$, are consistent throughout unless explicitly stated otherwise. The main domain is divided into 5 overlapping subintervals. To validate the current methodology and confirm the accurateness of the

Table 1
Comparison of the computational values of Nusselt Number $(Re_L)^{-1/2}Nu_L$ against outputs from Ref.[24] for different values of Pras$Ri = 0$, $\beta = 0$, $K = 0$, $Sc = 0$, $Hs = 0$, $Nr = 0$, $R = 0$, $Ec = 0$, $M = 0$.

Pr	$-\theta'(0)$		
	Abbas et al.[24]	Magyari and Keller[25]	Current Result
1.0	0.9551	0.9547	0.954783
3.0	1.8121	1.8691	1.869073
5.0	2.5577	2.5001	2.500132
10.0	3.6868	3.6604	3.660372

Table 2
Convergence Error.

Iterations	E_f	E_θ	E_ϕ
1	6.009×10^{-1}	1.798×10^{-1}	4.575×10^{-1}
2	1.420×10^{-1}	1.752×10^{-1}	1.406×10^{-1}
3	9.979×10^{-3}	5.313×10^{-2}	1.568×10^{-2}
4	3.343×10^{-5}	1.429×10^{-2}	8.832×10^{-3}
5	8.518×10^{-9}	1.105×10^{-3}	8.910×10^{-4}
6	2.797×10^{-10}	6.058×10^{-6}	1.621×10^{-6}
7	9.542×10^{-10}	2.934×10^{-11}	9.574×10^{-12}
8	5.063×10^{-11}	3.410×10^{-13}	2.776×10^{-13}
9	6.644×10^{-11}	8.134×10^{-13}	8.986×10^{-13}
10	1.606×10^{-11}	4.144×10^{-13}	6.275×10^{-13}

Table 3
Residual error.

Iterations	$\| \mathrm{Res}(f) \|_\infty$	$\| \mathrm{Res}(\theta) \|_\infty$	$\| \mathrm{Res}(\phi) \|_\infty$
1	3.333×10^{-1}	4.243×10^{-2}	1.076×10^{-2}
2	1.634×10^{-2}	3.699×10^{-3}	1.361×10^{-1}
3	7.602×10^{-6}	2.486×10^{-6}	1.969×10^{-4}
4	1.239×10^{-12}	2.487×10^{-13}	1.073×10^{-7}
5	2.285×10^{-5}	8.127×10^{-14}	2.477×10^{-14}
6	5.049×10^{-13}	6.350×10^{-14}	1.985×10^{-14}
7	5.089×10^{-13}	7.416×10^{-14}	3.077×10^{-14}
8	4.710×10^{-13}	6.972×10^{-14}	1.783×10^{-14}
9	4.654×10^{-13}	9.015×10^{-14}	7.119×10^{-15}
10	6.388×10^{-13}	5.862×10^{-13}	7.296×10^{-15}

computational code, numerical results obtainable in **Table-1** are compared with those reported by Abbas et al. ,[24] and Magyari and Keller.[25] The consistency between our findings and those from previous studies affirms the reliability of our numerical approach and the validity of our code.

To establish the convergence of the solution technique, the solution errors that highlight differences between estimated function values across iterations are examined. Convergence is illustrated using the infinity norm, as shown in Table 2. Clearly demonstrated in Table 1, are convergence errors that are consistently decreasing in a monotonic fashion as the number of iterations upsurges, serving as confirmation of the convergence of the numerical scheme. Additionally, we assess the accuracy of our solution approach by evaluating residual errors of the functions after a specified number of iterations. This involves substituting the approximate solutions into Eqs. (14-16) and computing the infinity norm of the residual error, as obtainable in Table 3. Inspecting the table, it is detected that a monotonic decrease in the residual errors for velocity, temperature, and concentration as the number of iterations rises. The magnitudes of the residual error values provide insights into the accuracy of the numerical solution. Lower error norms correspond to a more accurate solution. In this case, all the error norms are relatively small even at the first iteration, suggesting a good initial guess and rapid convergence. By the 10th iteration, the error norms have further decreased by an order of magnitude, reaching the 10^{-13},10^{-14}, and 10^{-15} range for momentum, temperature, and concentration profiles correspondingly. This specifies a high degree of accuracy in the solution profiles for momentum, temperature, and concentration.

4.1. Variation of Richardson number

Fig. 2 deliberates the interpretation of the Richardson number on the momentum profile $f'(\eta)$ of the third-grade liquid. The dimensionless number Richardson number Ri symbolizes the relative importance of buoyancy to shear forces within the fluid of the grade fluid flow via an inclined elastic sheet. The behavior is deployed for the consideration of the profile within the range $0.1 < Ri < 7$.At Low Richardson number it is observed that the shear forces dominate over the buoyancy forces which lead to a higher fluid velocity closer to the stretching sheet. However, with increasingRi, buoyancy effects became more significant and that enhances the fluid momentum in comparison to the lower value of Ri. Further, for the high values ofRi, the buoyancy forces dominate and leading to a substantial augmentation in the fluid momentum for which

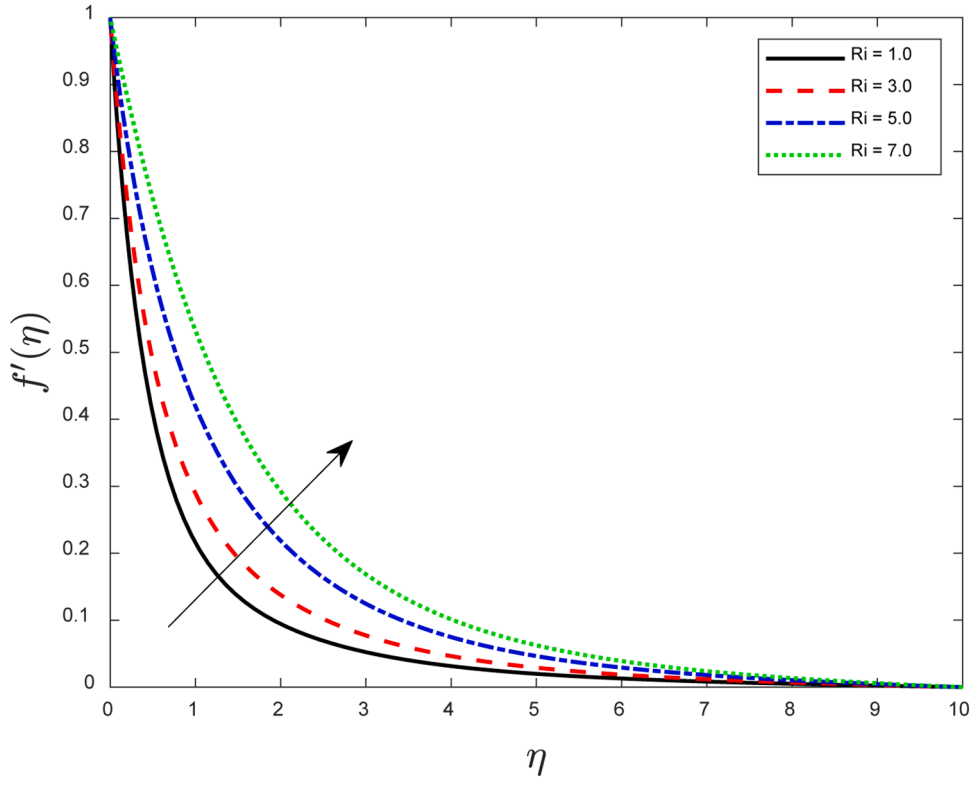


Fig. 2. $f'(\eta)$ varied against ηfor miscellaneous values of Ri.

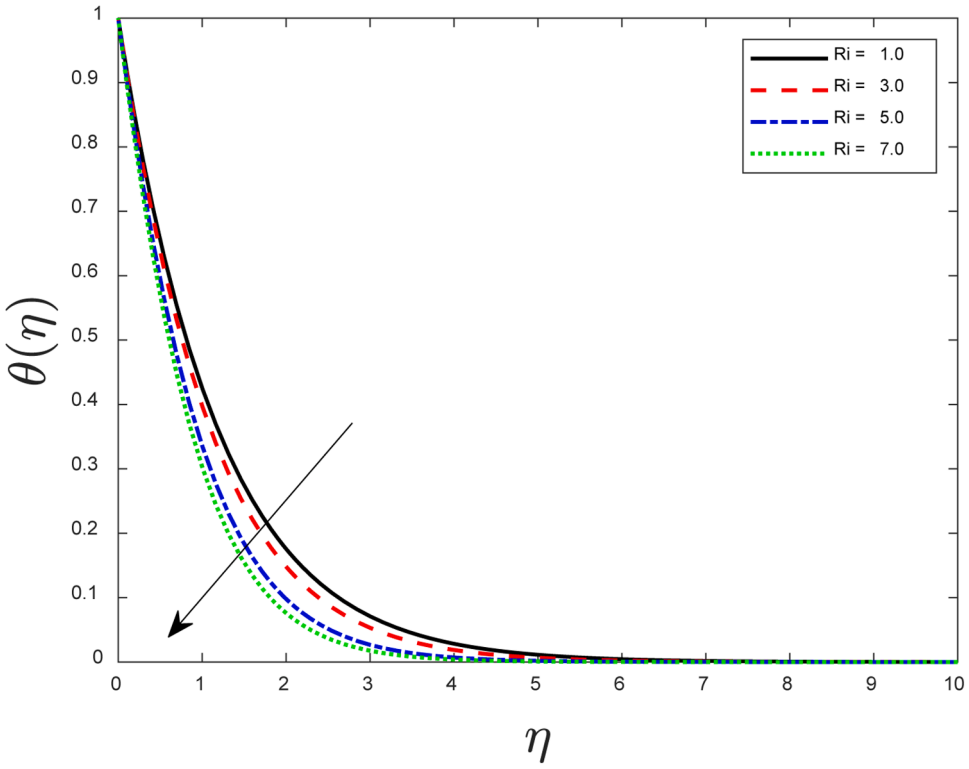


Fig. 3. θ(η) varied against ηfor miscellaneous values of *Ri*.

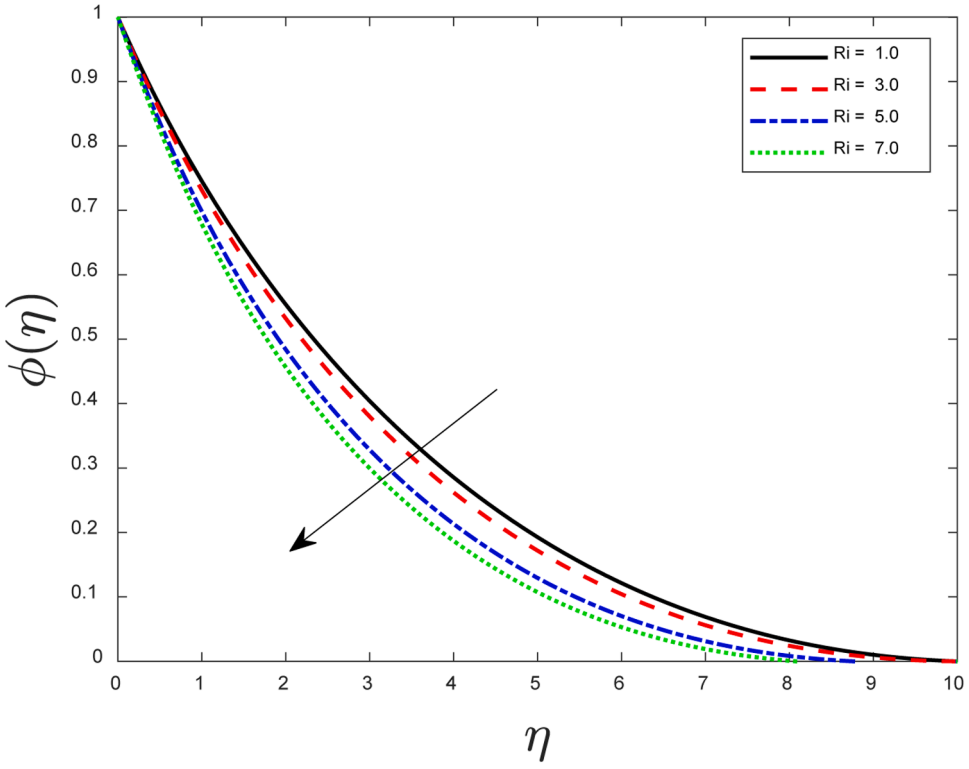


Fig. 4. ϕ(η) varied against η for miscellaneous values of*Ri*.

the bounding surface thickness increases significantly. Fig. 3 illustrates the insertion of *Ri* on the fluid temperature profile θ(η) of the non-Newtonian fluid. The minimal buoyancy effect for the low value of the *Ri*give rise to maximum temperature within the domain but with increasing *Ri*where the high value of *Ri* the buoyancy dominates over the shear force. This causes a noteworthy retardation in the fluid temperature θ(η) throughout. Irrespective to the variation of the Richardson parameter the profile is asymptotic in nature to meet the requisite

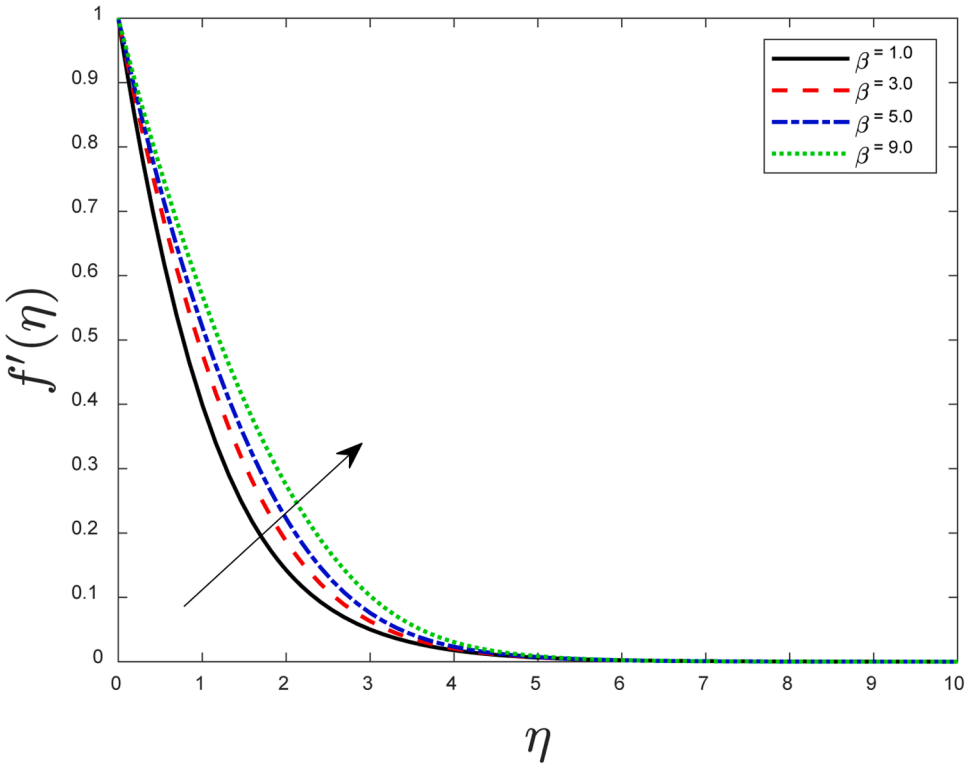


Fig. 5. $f'(\eta)$varied against ηfor miscellaneous values ofβ.

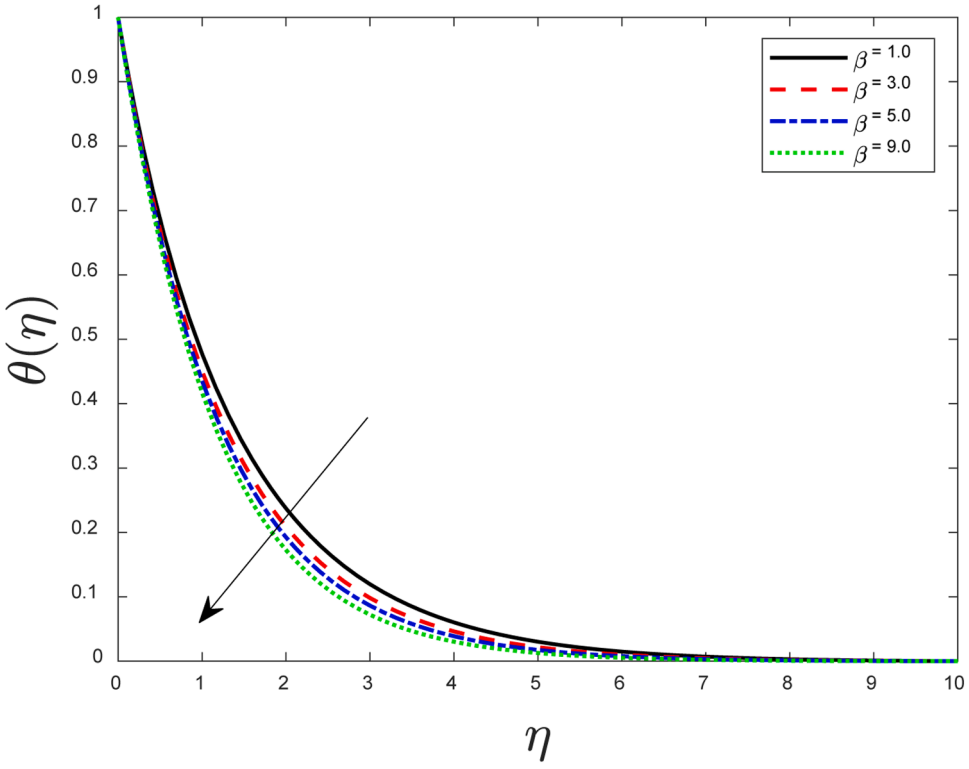


Fig. 6. θ(η)varied against ηfor miscellaneous values ofβ.

surface limitations. Fig. 4 illustrates the variation of *Ri* on the profiles of fluid concentration ϕ(η). The concentration profiles are more pronounced and influenced by the molecular diffusion with reaction rate for the lower values of the Richardson number. Further increasing *Ri*shows the greater impact of the buoyancy on the mass tranportation. This lead to a lower concentration gradient as buoyant forces aid in the dispersion of reactants. Therefore, high values of *Ri* resulting in a significantly reduced concentration gradient near the surface region.

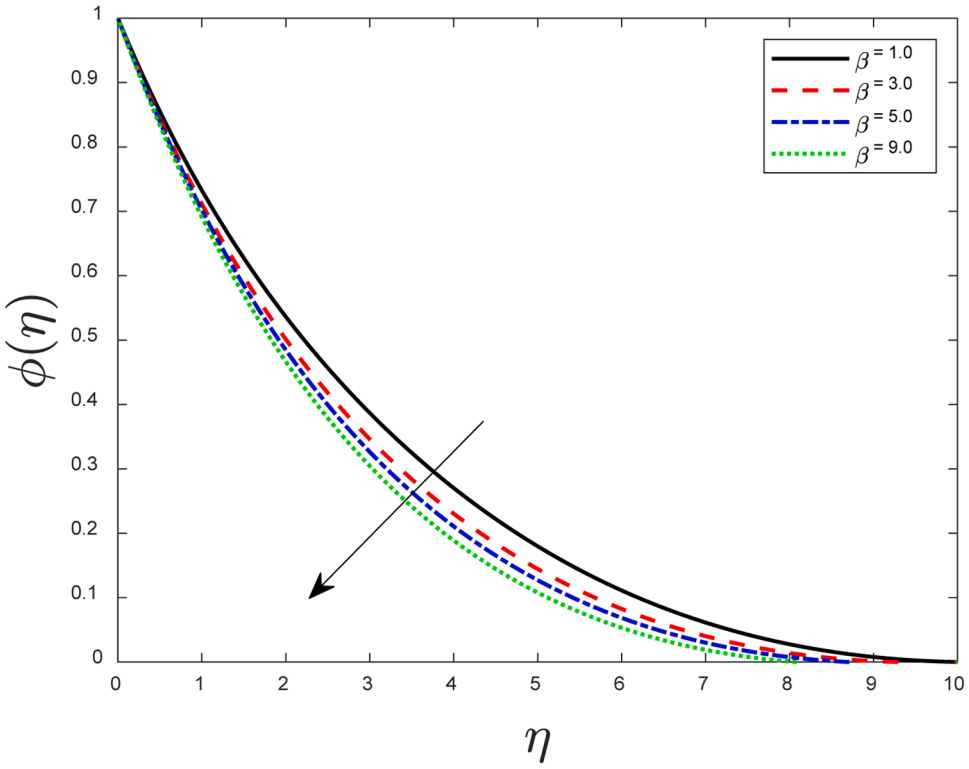


Fig. 7. ϕ(η)varied against ηfor miscellaneous values ofβ.

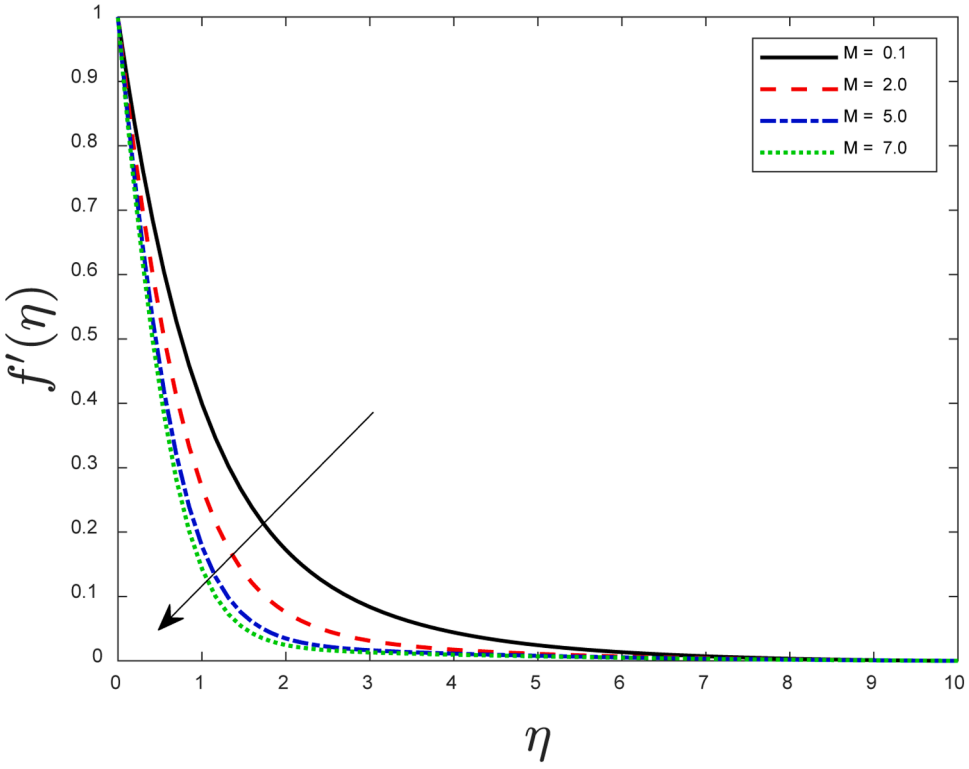


Fig. 8. $f'(\eta)$ varied against ηfor miscellaneous values of*M*.

4.2. Variation of third-grade parameter

The significant impact of third-grade factor on the fluid momentum profile $f'(\eta)$ which is depicted through Fig. 5. The impact is depicted for the motion of non-Newtonian fluid over an expanding surface where the inclined surface also plays vital role on the profile behavior. The distribution of the parameter is exhibited within the range described as$1 \leq \beta \leq 9$. Physically, the parameter b stands for the non-Newtonian features

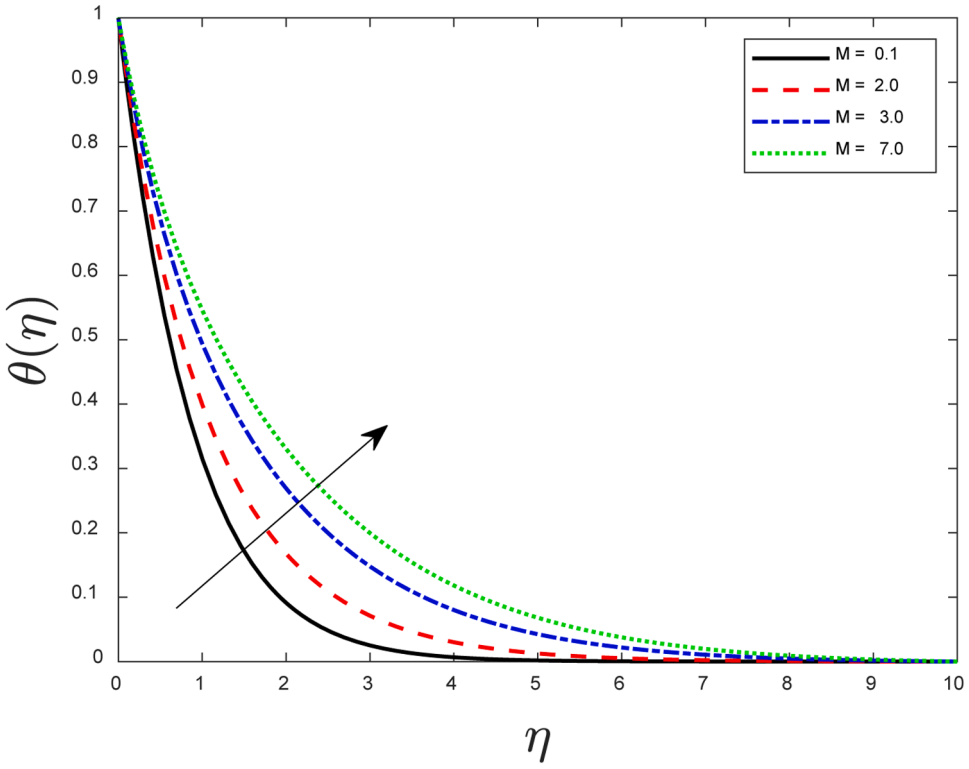


Fig. 9. θ(η)varied against ηfor miscellaneous values of*M*.

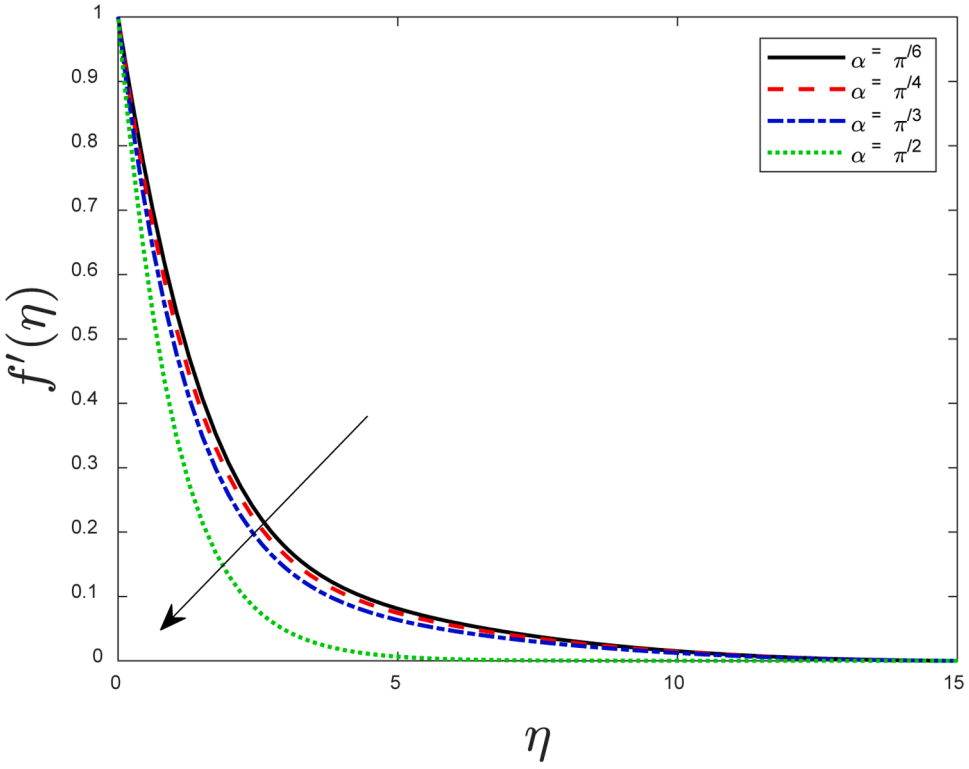


Fig. 10. $f'(\eta)$ varied against η for miscellaneous values ofα.

on the fluid profiles. Therefore, increasing b, the non-Newtonian characteristic of the fluid. The lower value of the β signifies the Newtonian property where the fluid velocity profile sees to βclose towards the sheet. Further, increasingβ, suggests an increase in the fluid resistance to enhanced deformation, which leading to a retarding fluid velocity. This is due to the enhanced nonlinear effects associated with higher-order fluid behavior. Fig. 6 describes the imposition of third grade factor on the fluid temperature θ(η) of the non-Newtonian fluid. The temperature

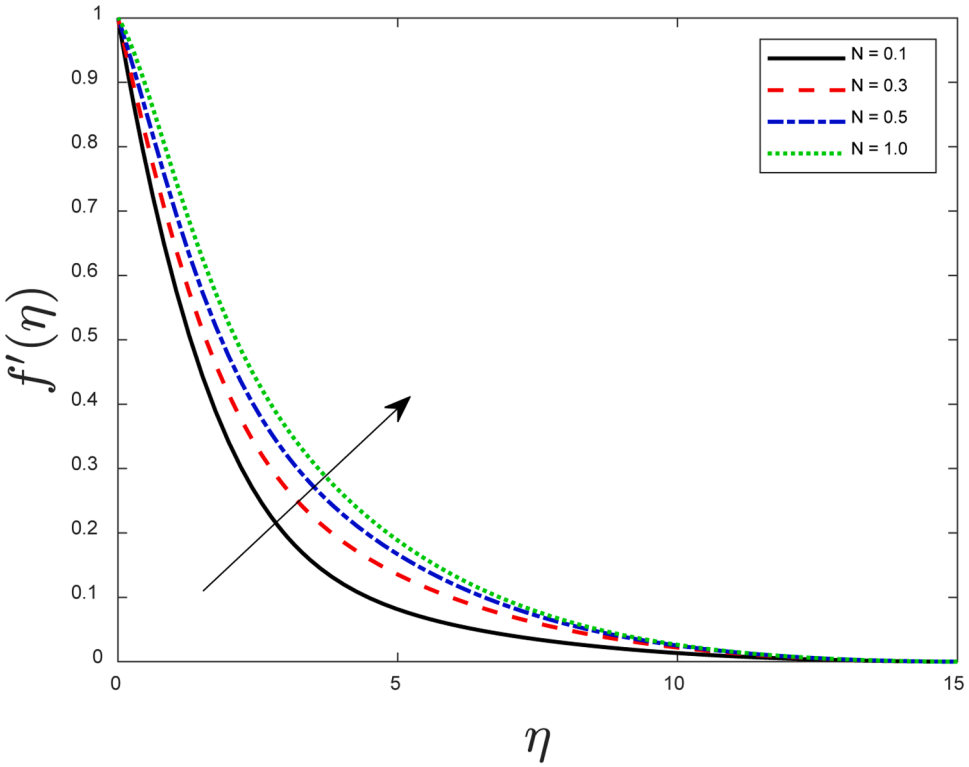


Fig. 11. $f'(\eta)$ varied against ηfor miscellaneous values of*N*.

distribution within the fluid is influence by both viscous dissipation with thermal radiation. The lower value ofβ, the rise in temperature is observed for the viscous dissipation is less significant. The higher values of theβshow a greater retardation in the temperature profile. Fig. 7 portrays the characteristic of third-grade parameter on the fluid concentration ϕ(η). In similar to the fluid temperature, it is disclosed that greater enhancing in the non-Newtonian parameter opposes the profile therefore the fluid concentration decreases significantly.

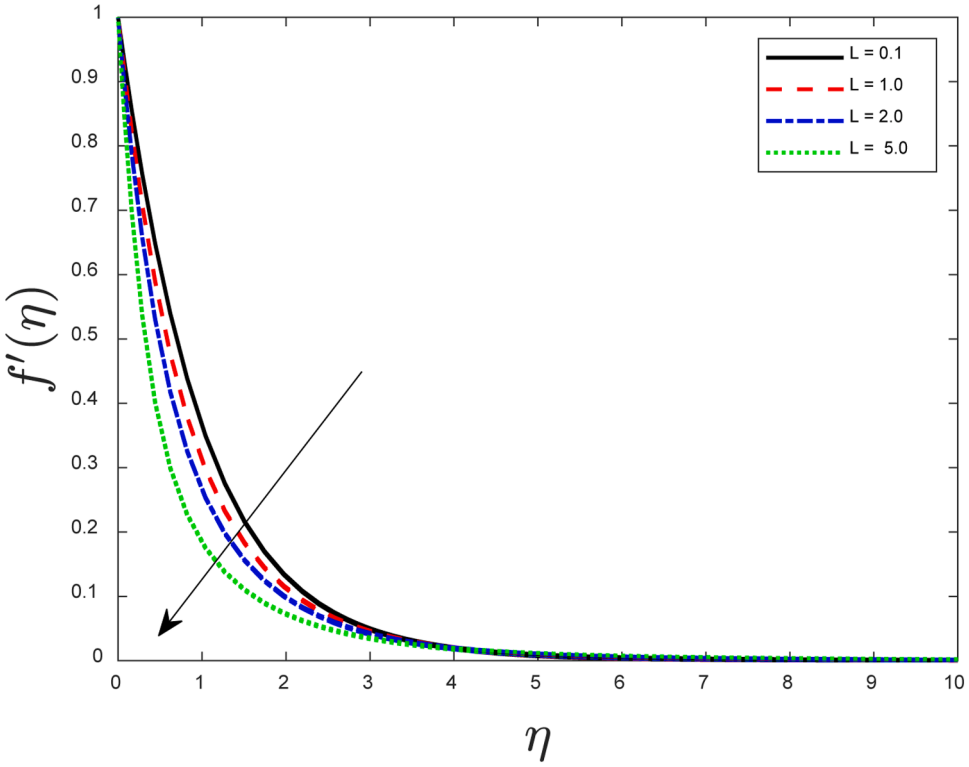


Fig. 12. $f'(\eta)$ varied against ηfor miscellaneous values of*L*.

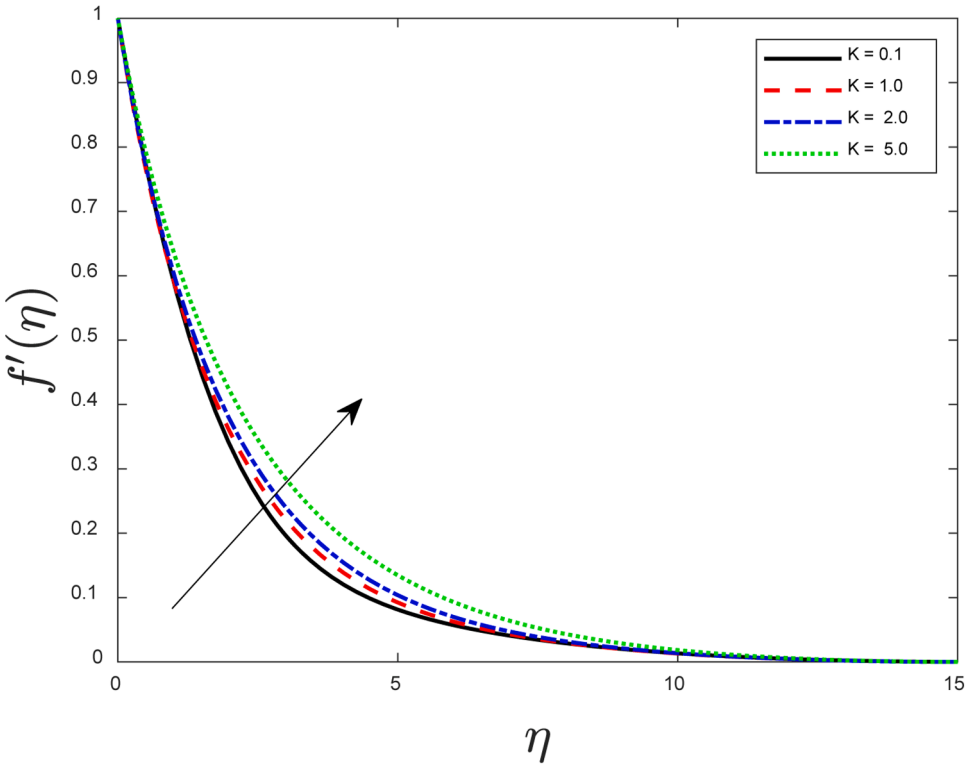


Fig. 13. $f'(\eta)$ varied against $\eta$for miscellaneous values of$K$.

4.3. Variation of magnetic parameter

Fig. 8 contributes the insertion of magnetization on the flow profiles and in particular showing on the velocity profile $f'(\eta)$ of the third-grade fluid. The imposition of magnetic factor which is projected due to the applied magnetic field acted along the transverse direction causes a resistive force. The variation is presented for the numeric values within the range 0.1 to 7. This significant characteristic is known as Lorentz force and the trend of this force is to resists the fluid momentum. It is seen that with the enhanced magnetization the profile strength retards.

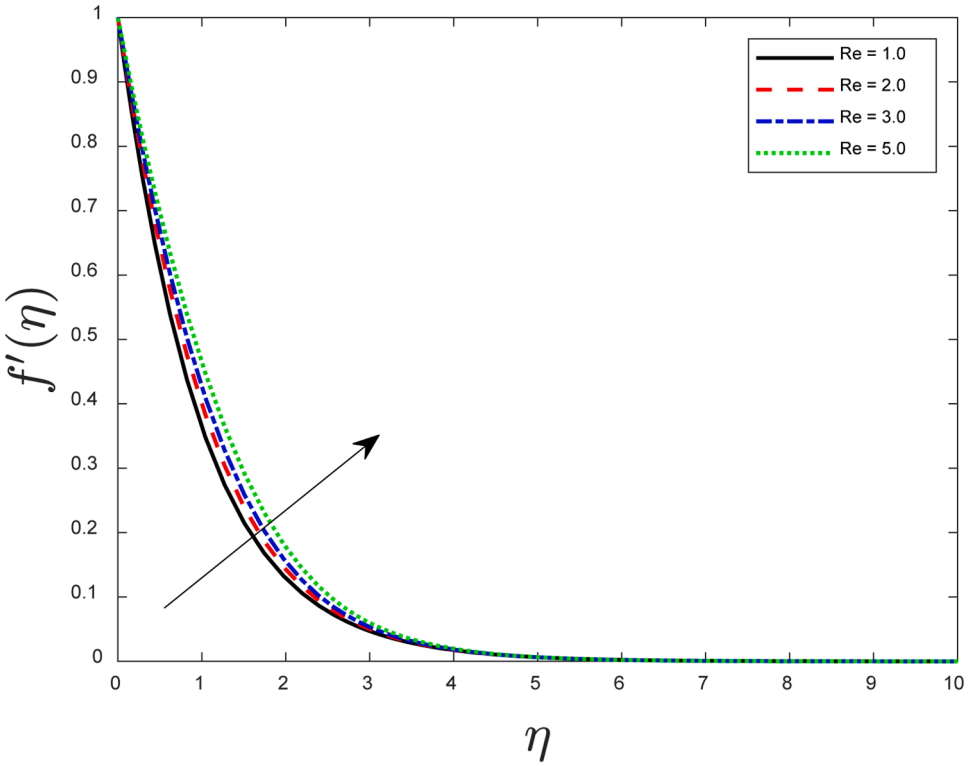


Fig. 14. $f'(\eta)$ varied against $\eta$for miscellaneous values ofRe.

This causes a noteworthy retardation in the profile thickness with respect to the bounding surface. Fig. 9 elaborates the dissimilar effect of the magnetic factor on the profile of fluid temperature θ(η) of the grade fluid through the inclined stretching surface. The behavior of the magnetization reveals a significant retardation in the velocity and that give rise to storage of energy near to the surface region. The stored energy then overshoots the heat energy from the solid surface via the fluid region. This characteristic suggests an enhanced temperature throughout the domain.

4.4. Variation of inclined angle and buoyancy ratio

Fig. 10 depicts the role of inclined angle of the surface on the fluid momentum distribution$f'(\eta)$. The range of the inclined angle (α)is restricted to $[\pi/6 - \pi/2]$. The sheet changes its position depending upon the variation of the inclined angle. Increasing inclined angle retards the fluid momentum. Therefore, the thickness of the bounding surface decreases significantly and the profile converges asymptotically to meet the adequate surface constraints. Fig. 11 contributes the association of buoyancy ratio factor on the fluid velocity$f'(\eta)$ with the presence of other characterizing factors involved in it. This impact is executed because of the nitration of both the thermal and solutal buoyancy on the fluid motion. The range of the parameter is suggested as $0.1 \leq N \leq 1$. The physical description reveals that, the increasing buoyancy ratio is due to the increasing solutal difference between the layers corresponding to the retardation in the surface force. This causes a difference in the density which contributes significant enhancing in the fluid velocity throughout.

4.5. Variation of viscoelastic parameter and cross viscous term

The combined effect of relaxation and retardation tie suggests the performance of the viscoelastic factor on the fluid motion $f'(\eta)$ which is depicted in Fig. 12. The low values of the viscoelastic factor indicate the behavior of the Newtonian case and the increasing values suggests the behavior is non-Newtonian. The graphical illustration displays that the growing elasticity attenuates the fluid momentum i.e., the Newtonian fluid dominates the behavior of the non-Newtonian irrespective to the variation of other characterizing factors. Fig. 13 illustrates the cross-viscosity factor on the fluid momentum $f'(\eta)$ of the non-Newtonian fluid. The increase in the viscosity significantly enhances the fluid momentum.

4.6. Variation of Reynolds number

Fig. 14 describes the insertion of the Reynolds number on the fluid velocity profiles $f'(\eta)$ of the non-Newtonian fluid past an inclined elongating surface. The dimensional parameter Re is the ratio of viscous an inertial force. The range of the factor is distributed within the range of $1 \leq \mathrm{Re} \leq 5$due to the occurrence of the other characterizing factors. The enhanced values of *Re* is because of the lower in the inertial force and this causes a significant enhancement in the fluid momentum. In addition to that the viscous force augments significantly showing an asymptotic nature of the profile to the requisite boundary conditions.

4.7. Variation of heat source

External heat sour is one of the factors which energies the fluid temperature profile of the viscoelastic fluid for the interaction of various characterizing factors. Fig. 15 demonstrations the significance of the contribution of heat source on the fluid temperature profile θ(η). The positive value of the factor signifies the external heat source applied on to the surface shows the energy flows outward from the lower region towards the fluid. This causes the energy transfer from the solid surface to liquid medium. Therefore, increasing heat source enhances the fluid temperature θ(η).

4.7.1. Variation of Eckert number and thermal radiation

Fig. 16 portrays the effect of coupling factor projected due to the insertion of Eckert number on the fluid temperature θ(η). The analysis of

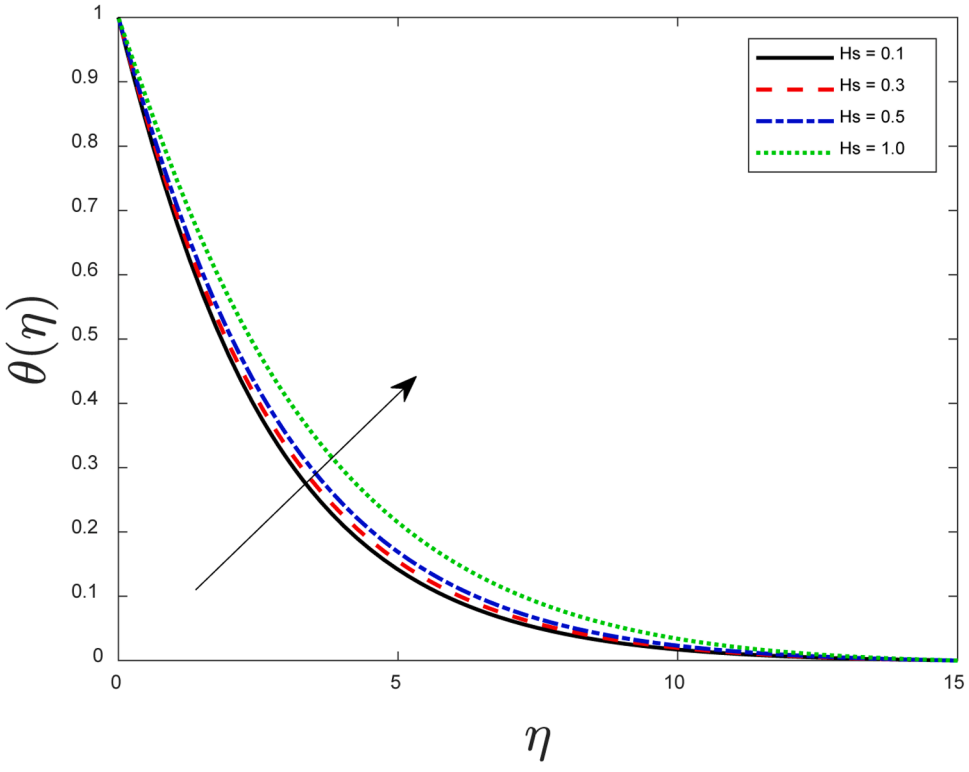


Fig. 15. θ(η)varied against η for miscellaneous values of*Hs*.

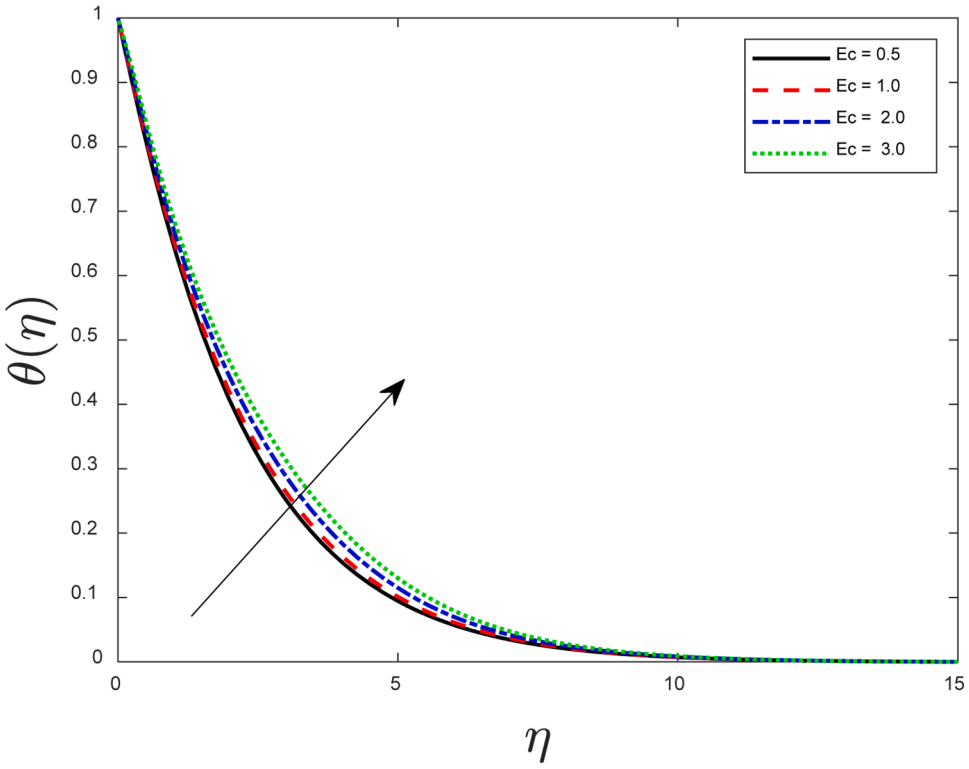


Fig. 16. θ(η)varied against η for miscellaneous values of*Ec*.

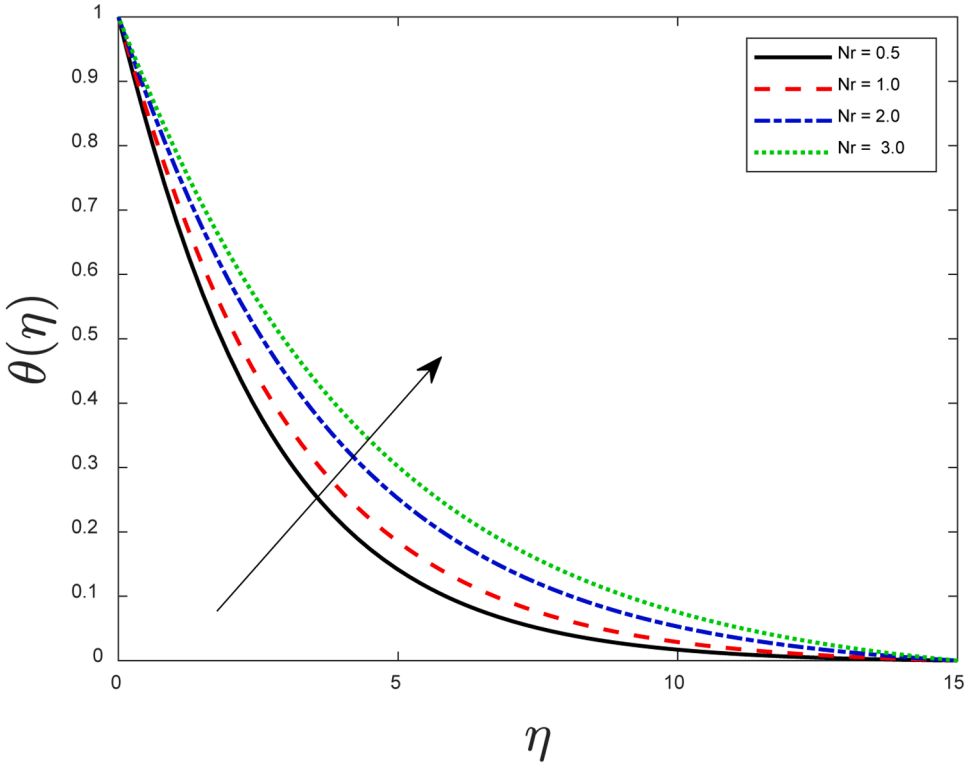


Fig. 17. θ(η)varied against η for miscellaneous values of*Nr*.

the Eckert number is obtaining for the consideration of the dissipative heat in particular the viscous dissipation in the energy equation. The dimensionless quantity physically expressed as the ratio of the kinetic energy with respect to the enthalpy change. The change in the values of the Eckert number is due to the change in enthalpy. Particularly, increasing *Ec* suggests that the change in the temperature difference retards. This causes a greater fluid temperature which is overrides the fact of ambient temperature and the propos phenomenon reveals that

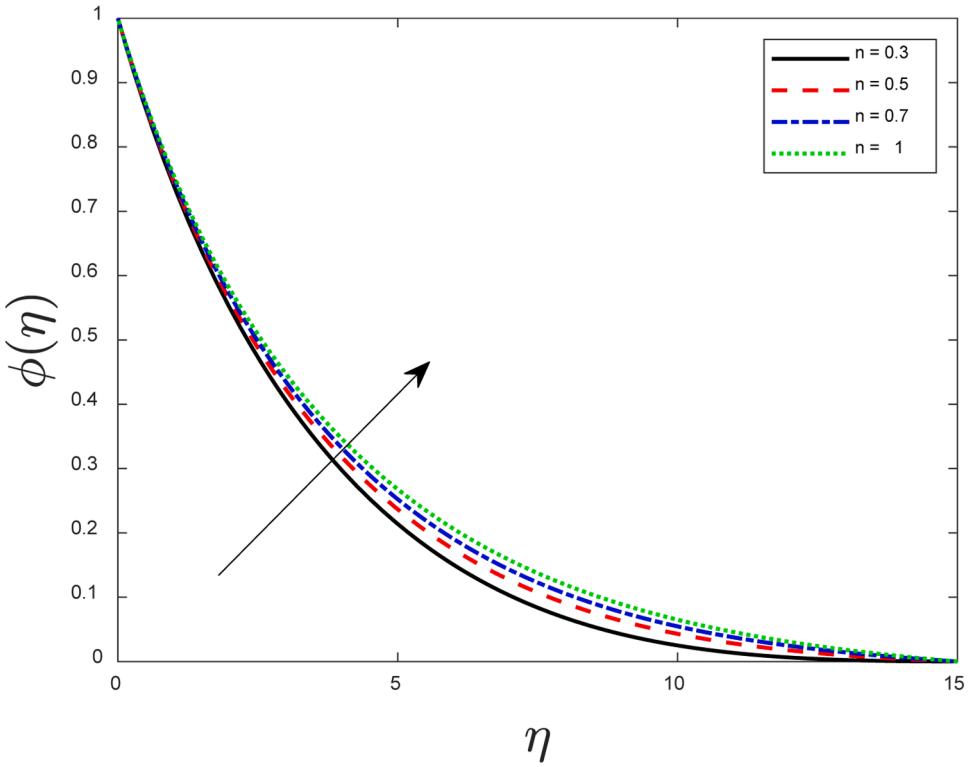


Fig. 18. ϕ(η)varied against ηfor miscellaneous values of n .

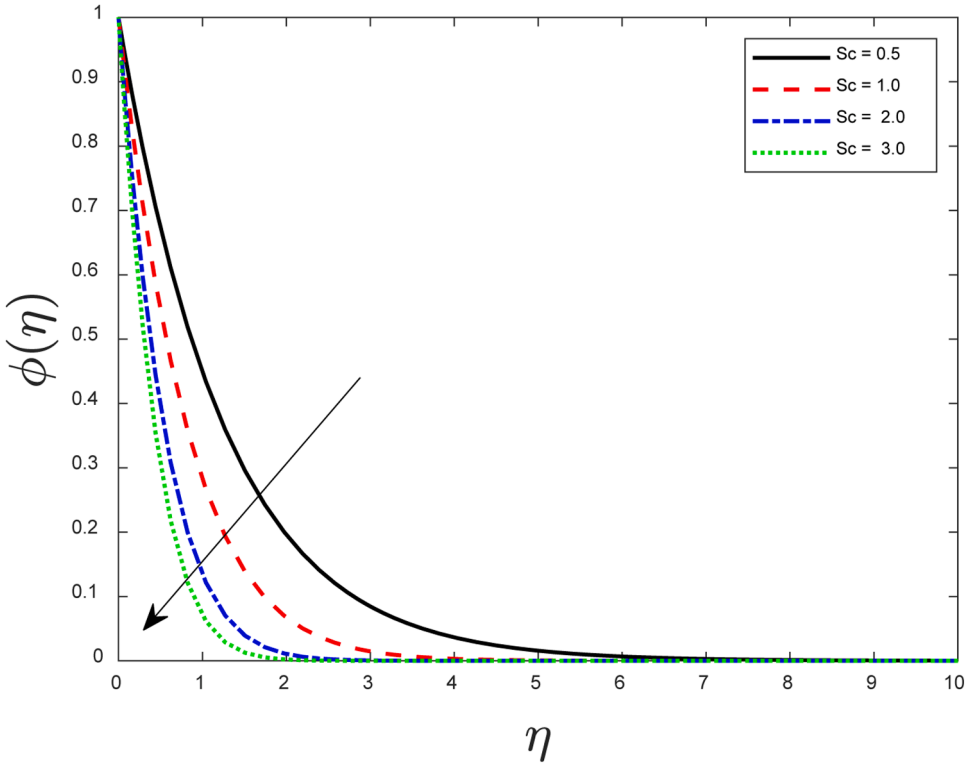


Fig. 19. ϕ(η)varied against η for miscellaneous values ofSc.

there is a flow of temperature from the surface region towards the fluid medium. This resulted in the fluid temperature increases significantly with a greater cooling of the surface. Further, Fig. 17 depicts the imposition of the radiant heat affecting the fluid temperature θ(η)of the non-Newtonian fluid. The factor Nr is the measure of the emission of the electromagnetic wave produced from the surface of the fluid increases. The transformation of the electromagnetic wave to the thermal radiation is obtained within the fluid medium and this causes a substantial change

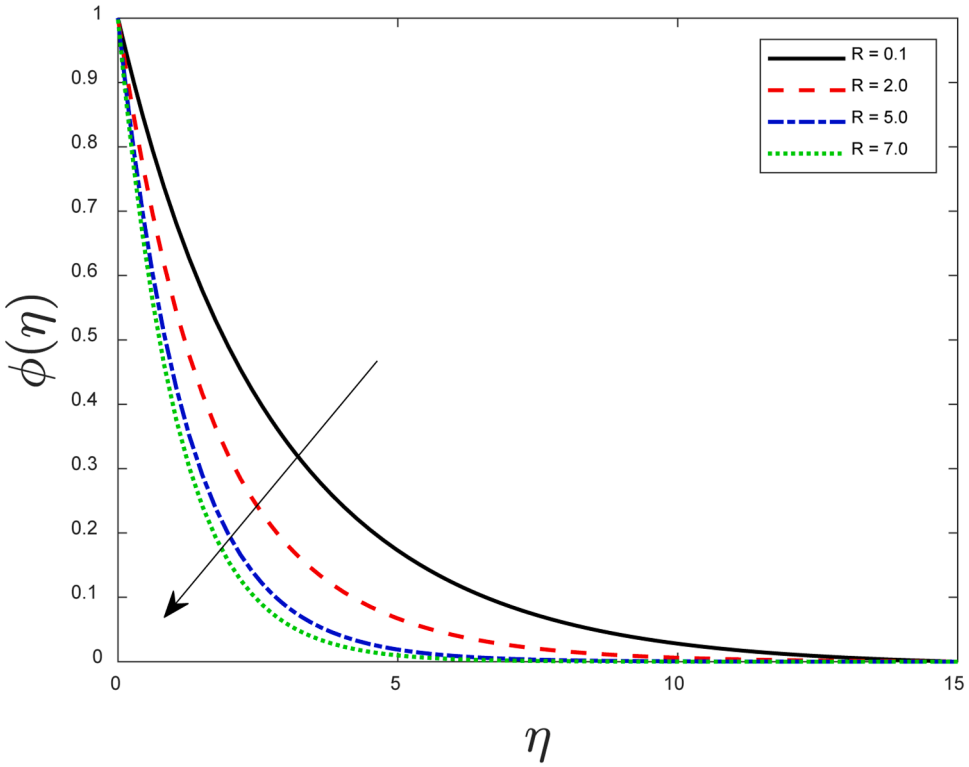


Fig. 20. ϕ(η)varied against ηfor miscellaneous values of*R*.

in the fluid temperature. The increasing Nr enhances the fluid departure significantly.

4.8. *Variation of different factors on concentration profile*

Fig. 18 demonstrations the role of power index factor on the fluid concentrationϕ(η). Power index described as the exponent variation of the chemical ration. Increasing the value of n suggest the significant retardation in the nanofluid concentration. Fig. 19 portrays the behavior of the *Sc*on the concentration profile. The Schmidt number is the ratio of the kinetic viscosity with respect to solutal diffusion. Therefore, increasing *Sc* retards the concentration due to the density of the heavier species. Fig. 20 illustrates the association of chemical reaction on ϕ(η) for the introduction of several gasses in to the system. The positive values of the chemical reaction show the destructive nature of the chemical reaction which also favors in decelerating concentration.

5. Conclusions

The free convection of a third-grade non-Newtonian fluid via an inclined elongating sheet is deployed in the current investigation. However, the flow phenomena became energies by integrating the influences of radiating heat and higher-order chemical reactions. The analysis also accounts for the effect of viscous dissipation on the heat transport phenomenon. The standard PDEs are converted into ODEs through appropriate similarity rules. These resultant ODEs are numerically unraveled utilizing the over lapping grid spectral quasilinearization method. The measure outcomes are depicted as;

- The quantitative result obtained for the particular case shows a good contract with the earlier work presenting the convergence analysis of the current methodology.
- A monotonic decrease in the residual errors for all the flow profiles is exhibited as the number of iterations increases.
- Richardson number which is conformed for the inclusion of thermal Grashof number exhibits a significant hike in the fluid momentum distribution but reverse impact is encountered for the temperature and concentration of the fluid.
- The third-grade parameter favors in enhancing the fluid velocity whereas the fluid temperature retards throughout with its increasing value.
- The resistive force that is generated from the imposition of uniform magnetic field significantly attenuates the fluid velocity but overshoots the fluid temperature.
- The increasing buoyancy ratio is due to the increasing solutal difference between the layers corresponding to the retardation in the surface force.
- Enhanced external heat source encourages the fluid temperature along with the increasing radiant heat and the Eckert number.
- Heavier species favorable in retarding the fluid concentration and the concentration profile is also controlled by the inclusion of reacting species.

Declaration of competing interest

The authors declare that they have no known competing financial interests or personal relationships that could have appeared to influence the work reported in this paper.

Appendix

Brief description of third grade fluid

The constitutive equation for a third-grade fluid is:

$$\tau = -pI + \mu_1 A_1 + \alpha_1 {A_1}^2 + \alpha_2 tr(A_1) A_1 + \beta_1 A_2 + \beta_2 A_3,$$

Where τIs the Cauchy stress tensor,*p*is pressure, *I* is the identity tensor, $\mu_1$is the fluid viscosity, α_1,α_2,β_1,$\beta_2$are the material constants, A_1,A_2,$A_3$are kinematic tensors of first, second and third grade fluids respectively.

Moreover, $A_1 = \nabla v + (\nabla v)^T$

$$A_2 = \frac{dA_1}{dt} + A_1 \cdot \nabla v + (\nabla v)^T \cdot A_1$$

$$A_3 = \frac{dA_2}{dt} + A_2 \cdot \nabla v + (\nabla v)^T \cdot A_2$$

Data availability

No data was used for the research described in the article.

Reference

1. Sandeep N, Sulochana C. Momentum and heat transfer behavior of Jefrey, Maxwell and Oldroyd-B nanofluids past a stretching surface with non-uniform heat source/sink. *Ain Shams Eng J*. 2018;9(4):517–524. https://doi.org/10.1016/j.asej.2016.02.008.
2. Abolbashari MH, Freidoonimehr N, Nazari F, Rashidi M M. Analytical modeling of entropy generation for Casson nanofluid flow induced by a stretching surface. *Adv Powder Technol* 26(2), 542–55. 10.1016/j.apt.2015.01.003.
3. Shit G C, Haldar R, Mandal S. Entropy generation on MHD flow and convective heat transfer in a porous medium of exponentially stretching surface saturated by nanofluids. *Adv Powder Technol*. 2017;28(6):1519–1530. https://doi.org/10.1016/j.apt.2017.03.023.
4. Ariel PD. Flow of a third-grade fluid through a porous fat channel. *Int J Eng Sci*. 2003;41(11):1267–1285. https://doi.org/10.1016/S0020-7225(02)00380-4.
5. Ellahi R, Riaz A. Analytical solutions for MHD flow in a third-grade fluid with variable viscosity. *Math Comput Modell*. 2010;52(9–10):1783–1793. https://doi.org/10.1016/j.mcm.2010.07.005.
6. Mahanthesh B, Joseph TV. Dynamics of magneto-nano third-grade fluid with Brownian motion and thermophoresis effects in the pressure type die. *J Nanofuids*. 2019;8(4):870–875. https://doi.org/10.1166/jon.2019.1642.
7. Pattnaik PK, Mishra SR, Sharma RP. Numerical simulation for flow through conducting metal and metallic oxide nanofuids. *J Nanofuids*. 2020;9(4):354–361. https://doi.org/10.1166/jon.2020.1753.
8. Pattnaik P K, Pattnaik JR, Mishra SR, Nisar KS. Variation of the shape of Fe3O4-nanoparticles on the heat transfer phenomenon with the inclusion of thermal radiation. *J Term Anal Calorim*. 2022;147(3):2537–2548. https://doi.org/10.1007/s10973-021-10605-9.
9. Anwar T, Kumam P, Watthayu W. Unsteady MHD natural convection flow of Casson fluid incorporating thermal radiative flux and heat injection/suction mechanism under variable wall conditions. *Sci Rep*. 2021;11(1):4275. https://doi.org/10.1038/s41598-021-83691-2.
10. Anwar T, Kumam P, Baleanu D, Khan I, Tounthong P. Radiative heat transfer enhancement in MHD porous channel flow of an Oldroyd-B fluid under generalized boundary conditions. *Phys Scr*. 2020;95(11), 115211. https://doi.org/10.1088/1402-4896/abbe50.
11. Anwar T, Kumam P, Khan I, Tounthong P. Fractional magnetohydrodynamic flow of a second grade fluid in a porous medium with variable wall velocity and Newtonian heating. *Fractals*. 2021;29(03), 2150060. https://doi.org/10.1088/1402-4896/abbe50.
12. Reddy G J, Hiremath A, Kumar M. Computational modeling of unsteady third-grade fluid flow over a vertical cylinder: a study of heat transfer visualization. *Results Phys.2018*. 2018;8:671–682. https://doi.org/10.1016/j.rinp.2017.12.054.
13. Baithalu R, Mishra SR, Pattnaik PK, Panda S. Optimizing shear and couple stress analysis for the magneto-micropolar dissipative nanofluid flow toward an elongating surface: a comprehensive RSM-ANOVA investigation. *J Therm Anal Calorim*. 2023;149:1697–1713. https://doi.org/10.1007/s10973-023-12741-w.
14. Mishra A, Upreti HA. Comparative study of Ag–MgO/water and Fe3O4–CoFe2O4/EG–water hybrid nanofluid flow over a curved surface with chemical reaction using Buongiorno model. *Partial Differ Eq Appl Math*. 2022;5, 100322. https://doi.org/10.1016/j.padiff.2022.100322.
15. Mishra A, Kumar M. Velocity and thermal slip effects on MHD nanofluid flow past a stretching cylinder with viscous dissipation and Joule heating. *SN Appl Sci*. 2020;2:1350. https://doi.org/10.1007/s42452-020-3156-7.
16. Mishra A, Rawat SK, Yaseen M, Pant M. Development of machine learning algorithm for assessment of heat transfer of ternary hybrid nanofluid flow towards three different geometries: Case of artificial neural network. *Heliyon*. 2023;9:11. https://doi.org/10.1016/j.heliyon.2023.e21453.
17. Aly EH, Rosca AV, Rosca NC, Pop I. Convective heat transfer of a hybrid nanofluid over a nonlinearly stretching surface with radiation effect. *Mathematics*. 2021;9:2220. https://doi.org/10.3390/math9182220.
18. Akram J, Akbar NS, Tripathi D. A theoretical investigation on the heat transfer ability of water-based hybrid (Ag–Au) nanofluids and Ag nanofluids flow driven by electroosmotic pumping through a microchannel. *Arab J Sci Eng*. 2021;46(3):2911–2927. https://doi.org/10.1007/s13369-020-05265-0.
19. Alhussain ZA, Tassaddiq A. Thin film blood based Casson hybrid nanofluid flow with variable viscosity. *Arab J Sci Eng*. 2022;47(1):1087–1094. https://doi.org/10.1007/s13369-021-06067-8.
20. Wang F, Nazir U, Sohail M, El-Zahar ER, Park C, Thounthong P. A Galerkin strategy for tri-hybridized mixture in ethylene glycol comprising variable diffusion and thermal conductivity using non-Fourier's theory. *Nanotechnol Rev*. 2022;11(1):834–845. https://doi.org/10.1515/ntrev-2022-0050.
21. Singh SP, Upreti H, Kumar M. Stagnation point flow of hybrid nanofluid driven towards a sinusoidal-radius permeable circular cylinder. *Int J Modell Simul*. 2024:1–13.
22. Maheshwari S, Bisht A, Upreti H. Bioconvective flow of thermally radiative Casson nanofluid with aerobic microorganisms over a stretching surface. *Chin J Phys*. 2024.
23. Singh SP, Upreti H, Kumar M. Investigating the quadratic convective flow attributes of radiative Casson hybrid nanofluid flow across cone and wedge using the Cattaneo-Christov model. *Numer Heat Transf Part B Fundamental*. 2024:1–24.
24. Abass A, Shafqat R, Jeelani MB, Alharti NH. Significance of chemical reaction and Lorentz force on third-grade fluid flow and heat transfer with darcy–forchheimer law over an inclined exponentially stretching sheet embedded in a porous medium. *Symmetry (Basel)*. 2022;14:779. https://doi.org/10.3390/sym14040779.
25. Magyari E, Keller B. Heat and mass transfer in the boundary layers on an exponentially stretching continuous surface. *J Phys*. 1999:32577–32585. https://doi.org/10.1088/0022-3727/32/5/012.
26. Mkhatshwa MP, Khumalo M. Entropy optimization in mixed convective boundary layer flow of CNTs Casson nanoliquid through a vertical cylinder moving with nonlinear velocity. *Int J Ambient Energy*. 2023;44:2569–2589. https://doi.org/10.1080/01430750.2023.2259400.
27. Basit M A, Imran M, Safdar R, Tahir M, Ali MR, Hendy A S, Alharthi AM. Thermally radiative bioconvective nanofluid flow on a wavy cylinder with buongiorno model: a sensitivity analysis using response surface methodology. *Case Studies in Therm Eng*. 2024, 104178. https://doi.org/10.1016/j.csite.2024.104178.
28. Oluwaseun F, Goqo S, Mondal H. Unsteady squeezing flow and heat transport of SiO2/kerosene oil nanofluid around radially stretchable parallel rotating disks with upper disk oscillating. *Propuls Power Res*. 2024;13(1):64–79. https://doi.org/10.1016/j.jppr.2024.02.005.